Electrochimica Acta 320 (2019) 134544

Contents lists available at ScienceDirect

Electrochimica Acta

journal homepage: www.elsevier.com/locate/electacta

Efficient photocatalysis through conductive polymer coated FTO counter electrode in platinum free dye sensitized solar cells

Shehna Farooq [a], Asif Ali Tahir [b], Ulrike Krewer [c], Anwar ul Haq Ali Shah [d], Salma Bilal [a, c, *]

[a] National Centre of Excellence in Physical Chemistry, University of Peshawar, 25120, Peshawar, Pakistan
[b] Environment and Sustainability Institute (ESI), University of Exeter, Penryn Campus, Penryn, Cornwall, TR10 9FE, United Kingdom
[c] TU Braunschweig Institute of Energy and Process Systems Engineering, Franz-Liszt-Straße 35, 38106, Braunschweig, Germany
[d] Institute of Chemical Sciences, University of Peshawar, 25120, Peshawar, Pakistan

ARTICLE INFO

Article history:
Received 13 March 2019
Received in revised form
9 July 2019
Accepted 13 July 2019
Available online 17 July 2019

Keywords:
Photocatalysis
Dye sensitized solar cells
Pani
Counter electrodes
Solar energy
Ammonium lauryl sulphate

ABSTRACT

Platinum-free counter electrodes are crucial for developing cost effective solar energy harvesting technology. We describe here the fabrication of efficient platinum free FTO counter electrodes for dye sensitized solar cells based on pristine polyaniline, polyaniline doped with sulfuric acid, ammonuim lauryl sulfate, as well as binary doped with sulfuric acid and ammonium lauryl sulphate. The characteristics of these counter electrodes were analyzed using cyclic voltammetry, photocurrent density −voltage and electrochemical impedance spectroscopy measurements. At optimized fabrication conditions, the counter electrode shows significantly high photoelectric conversion efficiency of 4.54% compared to 4.03% for reference platinum counter electrode. Charge transfer resistance at the interface between electrolyte and counter-electrode is also decreased for the optimized polyaniline based counter electrode. Furthermore, the device presented characteristics of multiple start/stop ability and fast activity. The simple preparation procedure, low cost and improved photoelectric properties permit fabricated counter electrode to be a reliable alternative for dye sensitized solar cells.

1: Introduction

Environmental pollution and increasing energy demands have incited research on clean and renewable energy sources. One of the most profitable renewable energy is solar energy because it is inexhaustible, and is environment friendly. In 1991 Gratzel developed a highly efficient Dye Sensitized Solar Cell (DSSC) encouraging a drift of research related to DSSCs [1,2] This was considered as a technically and economically credible alternative to traditional silicon solar cells owing to the low material cost, easy and inexpensive fabrication methods and competitive light to current conversion efficiencies [3,4].

A standard DSSC is fabricated by utilizing three major components: a porous film of TiO_2 sensitized by dye as an anode, an electrolyte solution containing iodide redox system between the electrodes, and platinized fluorinated tin oxide (FTO) glass substrate as a counter electrode (CE). CE is a significant constituent of DSSC and is responsible to provide electrons for the I^-/I_3^- redox couple in the electrolyte [5]. Normally platinum loaded FTO is utilized as a CE inferable from its higher electro catalytic activity for I_3^- to I^- redox couple. However, Pt metal is undoubtedly expensive and its cost as a CE is over 40% of the whole DSSC [6]. Moreover, Pt requires high energy for preparation and is susceptible to corrosion by tri iodide electrolyte. These defects directly make Pt unfavorable for durable stability and practical manufacture of DSSCs. Subsequently, the substitution of Pt by an alternative material remains a serious matter in DSSCs development [7]. Considering these defects, it is essential to substitute easily fabricated, stable and cost effective platinum free counter electrodes in DSSCs. Several materials such as derivatives of carbon (graphene based carbon [8], carbon nanotubes [9], carbon nanofibers [10], etc.), metal alloys [11], transition metal compounds [12,13] and intrinsically conductive polymers (ICPs) [1,6] have been investigated for the replacement of Pt. However, various draw backs such as low stability, low catalytic activity and low efficiency, have been reported among most of these candidates. However, conductive polymers in DSSCs are more desirable as CE catalysts due to their facile synthesis, porous structure, electrical conductivity, low cost, abundance, and

* Corresponding author., TU Braunschweig Institute of Energy and Process Systems Engineering, Franz-Liszt-Straße 35, 38106, Braunschweig, Germany.
E-mail addresses: s.bilal@tu-braunschweig.de, dresalmabilal@gmail.com (S. Bilal).

https://doi.org/10.1016/j.electacta.2019.07.055

favorable catalytic properties [14]. The most adopted conductive polymers as counter electrode for DSSCs include Polypyrrole (PPy), Poly (3,4-ethylenedioxy-thiophene) (PEDOT), and Polyaniline (Pani). They have attracted much interest as alternative CEs in DSSCs due to the ambient temperatures used in their synthesis as well as conducting nature and facile deposition methods [15]. As PPy has the problem of low stability and PEDOT is costly, Pani can be considered as an encouraging state-of-the-art-material to replace Pt CE in a DSSC due to its superior electro catalytic activity, stability and availability of various simple and cost effective routes for its synthesis [1].

The synthesis routes may include enzymatic, electrochemical, template and chemical oxidative methods [1,16,17]. Pani prepared by an efficient and versatile in situ chemical oxidative polymerization method is proven to be effective method for its utilization in sensors [18], supercapacitors [19] and DSSC [20].

Various studies have been reported for the preparation of Pani films through both chemical and electrochemical methods and to assess the capability of Pani as a CE for solar cell applications [1,6,21]. However, the performance of DSSC using these Pani CEs is still low as compared with that of Pt CE [14]. Therefore, a further improvement of its electro catalytic performance and efficiency is a requisite.

Pani is distinctive in that its metallic states can be reversibly controlled through charge-transfer doping and protonation. Its electrochemical properties can readily be tuned by controlled doping. The incorporation of a dopant in synthetic mixture can significantly alter the electrical and morphological properties of the synthesized polymers [22–24].

A CE with high electrocatalytic activity, electric conductivity and fine transparency in visible and near-infrared region, low band gap, high thermal and chemical stability and processability can overcome the issue of high charge transfer resistance (Rct) which is an important factor to improve the performance of DSSCs [25]. Therefore, it is crucial to improve the electro chemical and optical properties of Pani CE such as desirable band gap processability, electric conductivity and elecrocatalytic activity [26,27]. In order to improve the above mentioned properties, some effective approaches have been implemented by adding different organic and inorganic dopants into Pani matrix such as sodium fluoroacetate [28], camphor sulfonic acid (CSA) [29], sulphuric acid (H_2SO_4) [6] and sodium dodecyl sulfate [21].

It has been recognized that organic dopants may increase the stability and processability of Pani. While inorganic acids are reported to decrease the band gap. As a result the conductivity of Pani is increased through creation of various degrees of charge delocalization on the polymer backbone [30]. Yin Qiu fabricated Pani CEs for DSSCs in the presence of sodium dodecyl sulfate with improved conductivity and electrocatalytic activity, resulting in an enhanced efficiency [21]. Wang et al. studied the effect of sulphuric acid on the properties of Pani CE. They found great influence of dopant on the performance of resultant DSSCs [6].

Herein, we have adopted a strategy to binary doped Pani with H_2SO_4 and ammonium lauryl sulfate (ALS) with the aim to develop efficient and cost effective materials. ALS was used as a novel dopant. The synthesis of binary doped Pani (P-Mix) was carried out via chemical oxidation polymerization and its photocatalytic properties were analyzed and utilized for efficient Pt-free CE in DSSCs. In addition, the effect of H_2SO_4 and ALS on electrocatalytic activity, photovoltaic performance as well as charge transport properties was investigated. Furthermore, performance of the DSSCs based on P-Mix was compared with those based on Pt CE, Pristine Pani (P–N), ALS doped Pani (P-ALS) CE and H_2SO_4 doped Pani (P–H_2SO_4) CE. So far no work is reported about the Pani CEs prepared with such surfactant/dopant combination for DSSCs application.

2: Experimental

2. 1: Materials

Aniline (ANI), Ammonium Lauryl Sulphate (ALS), Dimethyl formamide (DMF), N-Methyl-2-pyrrolidone (NMP), Dimethyl sulfoxide (DMSO) were obtained from Acros. ANI was distilled prior to use and stored in the refrigerator. Chloroform was purchased from Scharlau chemicals. Ammonium per Sulphate (APS) was provided by Merck and Sulphuric acid (H_2SO_4) from Sigma Aldrich.

Anhydrous lithium iodide (LiI), Iodine (I_2), 3-methoxypropionitrile (MPN), 4-tert-butylpyridine (TBP), deoxycholic acid (DCA) and 1,2-dimethyl-3-propylimidazolium iodide (DMPImI), were obtained from Aldrich. TiO_2 (20 nm), Fluorine-doped Tin Oxide (FTO) glass (13 Ω/sq), 25 μm of surlyn and Rhothenium Dye D179 (Di-tetrabutylammonium cis-bis(isothiocyanato) bis(2,2-bipyridyl-4,4-dicarboxylato)ruthenium(II)) were obtained from Solaronix.

2. 2: Synthesis of binary doped pani

The chemical polymerization of binary doped Pani was carried out by adding 0.0098 mol of aniline to 0.62 mol of chloroform in a round bottom flask under constant stirring at room temp following by the addition of 0.008 mol of ALS. After this, 0.0012 mol of H_2SO_4 and APS solutions, dissolved in 100 ml water, were dropwise added in the above mixture, respectively. The mixture turned green with time showing formation of Pani. After 24 h the reaction was stopped, Pani was separated from this mixture through a separatory funnel and washed copiously with distilled water and acetone. The obtained Pani powder was dried in vacuum.

2. 3: Synthesis of H_2SO_4 doped pani, ALS doped pani and Pristine Pani

For comparative purpose, Pani doped alone with H_2SO_4 or ALS and Pristine Pani without ALS and H_2SO_4, were synthesized under the same conditions as mentioned above.

These polymers along with their codes are shown in Table 1.

2. 4: Fabrication of pani based counter electrodes (CEs)

In a series of experiments, P–N, P–H_2SO_4, P-ALS and P-Mix in the form of powder were dispersed in NMP at a constant concentration (0.5 g/ml) under stirring for 2 h. The dispersed Pani solutions were deposited on the FTOs by Doctor blade technique [5] and dried at 50 °C for 10 min. The thickness of all the films was about 8 μm (Fig. 1 e). Prior to this, FTO coated glass substrates were ultrasonically cleaned with deionized water, acetone, and 2-propanol for 15 min in each round. The Pt CE was prepared by thermal decomposition of H_2PtCl_6 on FTO substrates for 30 min at 385 °C.

Table 1
Pani samples and their codes.

Samples Name	Code
Pristine Pani	P–N
H_2SO_4 doped Pani	P–H_2SO_4
ALS doped Pani	P-ALS
ALS – H_2SO_4 doped Pani	P-Mix

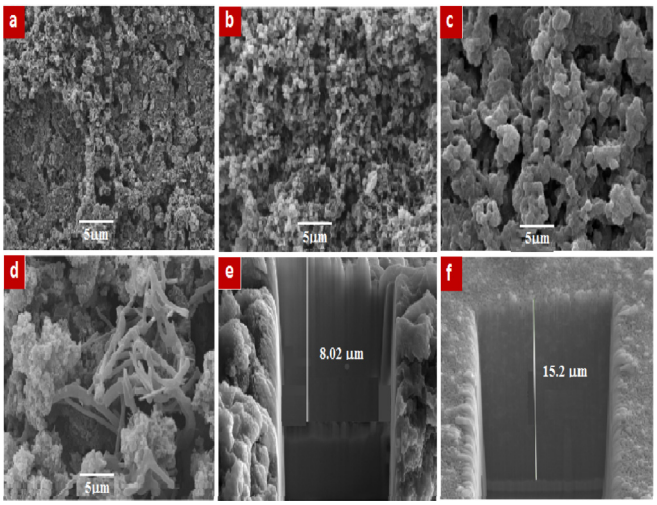

Fig. 1. Top view of SEM of a) P–N b) P–H_2SO_4 c) P-ALS and d) P-Mix. (e and f) FIB-SEM cross sections of P-Mix and TiO_2 films, respectively.

2. 5: Fabrication of DSSCs devices

Different layers of 20 nm opaque TiO_2 (Dyesol 18NR-O) paste were deposited on FTO glasses using screen printing technique followed by rapid annealing at 150, 300, 350, 400, 450, and 500 °C for 10, 15, 10, 15, 10 and 15 min, respectively. The thickness and active area of the obtained TiO_2 photoanodes was about 15 μm and 0.28 cm^2, respectively as indicated in Fig. 1 f. After cooling down to 80 °C, they were dipped into ethanolic solution of N719 dye (0.5 mM) for 24 h followed by cool air drying. The as prepared Pani CEs were positioned over the sensitized TiO_2 electrodes with a surlyn between them by using paper clips (Scheme 1). A few drops of redox electrolyte comprising 0.04 M I_2, 0.4 M LiI and 0.4 M tetrabutylammonium iodide (TBAI) dissolved in 0.3 M N-methylbenzimidazole (NMB) in 3-methoxypropionitrile (MPN) and acetonitrile (ACN) mixture at a volume ratio of 1:1 were then carefully applied between the photoanodes and CEs. The excess electrolytes were removed by using clean wipes. The overall illustration is presented in Scheme 1.

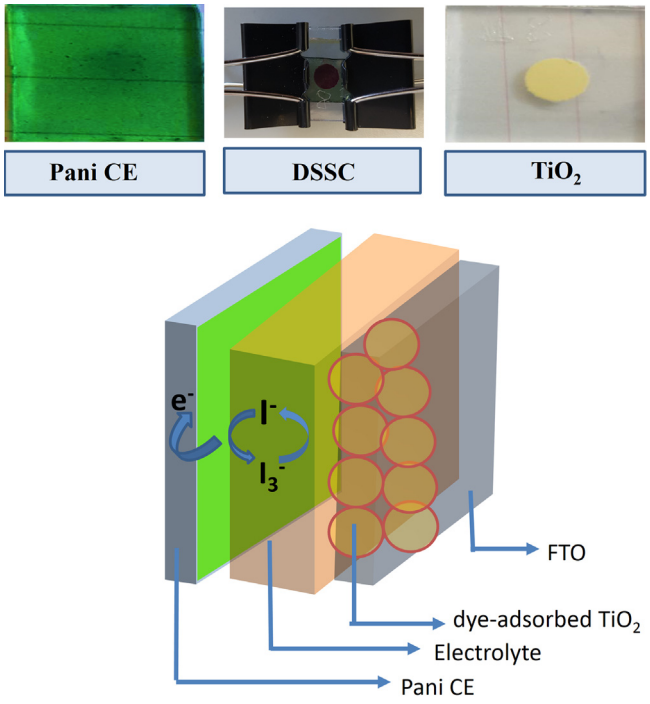

Scheme 1. Illustration of the representative structure of Pani CE for DSSCs.

2. 6: Characterization

The elemental mapping and surface morphologies of different Pani samples as well as morphologies of the counter electrodes were observed with SEM-EDX, SEM and FIB-SEM respectively (Helios G4 CX Dual Beam microscope equipped with Octane Elite). The structural information about all the synthesized samples were obtained through recording ATR-FTIR (Shimadzu) spectra in the range of 400–4000 cm^{-1}. The crystallinity of different samples of Pani was analyzed by using Rigaku X-Ray diffractometer (Japan) operated at 30 mA and 40 KV with wavelength of 1.5405 Å over the range of 10°–80°. For dc conductivity measurements, dry pellets of powder samples with 13 mm diameter and 5 mm thickness were prepared under a pressure of 20 MPa. Electrical conductivity of these pellets was tested by using Jandel RM3000 four-probe resistivity/square resistance tester at room temperature.

Absorption spectra were collected using a PerkinElmer spectrophotometer in NMP using scan range of 300–900 nm. To study the electro catalytic performance, CV measurements were conducted using Metrohm Autolab with Nova Software in redox electrolyte containing 0.1 M $LiClO_4$, 1.0 mM I_2 and 10 mM LiI in acetonitrile within the potential range of −0.6–1.2 V at various scan rates (30, 50, 75, 100, 125 mV/s). Pani/FTO or Pt/FTO were used as working electrode and Ag/AgCl and Pt wire were used as reference and counter electrodes, respectively. The constant quantity of synthesized materials were dissolved in NMP and drop coated on FTO glasses followed by drying at 50 °C for 5 min.

2. 7: Photoelectric characterization

The photovoltaic tests of Pristine Pani, doped Pani's and Pt based DSSCs were performed by measuring the photocurrent density-voltage (I–V) curves using the Metrohm Autolab with a light source of 100 W Xenon arc lamp in an ambient atmosphere. Current density and time curves of the DSSCs assembled with P-Mix CE were recorded by alternately irradiating (100 mW cm^{-2}) and darkening (0 mW cm^{-2}) the cell over 600 s to study the start/stop ability of the cell. Electrochemical impedance spectroscopy (EIS) of DSSCs were performed using the aforementioned Metrohm Autolab in ambient atmosphere under light with a frequency range of 0.01–10^5 Hz and 0.7 V bias. The obtained EIS spectra were simulated by Autolab impedance analyzer. Each I–V curve was repeatedly measured at least five time to control the experimental error within ±5%.

3: Results and Discussion

3. 1: SEM

Fig. 1 a-d, respectively, shows scanning electron micrographs of P–N, P– H_2SO_4, P-ALS and P-Mix. It can be observed that the counter ions derived from the dopants has significant influence on the morphological features of the resulting polymer. The morphological analysis reveals some fascinating features as a function of organic and inorganic acids used during synthesis.

The microstructure of P–N, as shown in Fig. 1a, seems to consist of closely packed aggregations probably due to intermolecular and intramolecular hydrogen bonding. This compact structure might increase interfacial and penetration resistance for charger transfer

and for exchange of I^-/I^-_3 redox couples [31]. P–H_2SO_4 (Fig. 2b) shows interconnected fibrous like morphology while P-ALS exhibits micro porous structure ((Fig. 2a and b). Interestingly, in the case of P-Mix (Fig. 2a and b) it is illustrious that some morphological features are similar to those of P– H_2SO_4 and P-ALS [32]. Short Pani nano fibers might grow on porous sites of ALS and long interconnected rod like morphology with porosity is thus observed in P-Mix [33]. This porous and rod like morphology of Pani can be considered beneficial to the diffusion and rapid exchange of I_3^- redox couples within the CE material [34].

Fig. 2a and b represent the FIB SEM cross sections of TiO_2 and P-Mix CEs. The thickness of TiO_2 film and P-Mix are 15.2 μm and 8.02 μm, respectively. Same thickness of other CEs is used in this study.

3. 2: XRD and FTIR analysis

The XRD diffraction patterns of P–N, P–H_2SO_4, P-ALS and P-Mix are shown in Fig. 2a. The Pani exhibits two significant peaks located at $2\theta = 20.2°$ and 25.2°, corresponding to the diffraction of crystallographic planes of Pani which originates from the main chains of the polymer structure. These peaks are recognized to the periodicity parallel and perpendicular to the Pani chain, respectively [35].

Similar peaks are also observed in all samples in addition to the shoulder peak at $2\theta = 14.4°$. This peak is considered to be specific for an anionic lattice and can be assigned to scattering from a lattice built up from main Pani chains [36]. With addition of binary dopant into the Pani, the diffraction peak becomes sharper, indicating a growth of composed crystallites [37]. The conversion of shoulder peak into intense peak in all doped samples suggests the incorporation of dopants induces ordered packing of polymer chains. All these peaks are symbolic of semi crystalline emeraldine salt of Pani [38].

The above discussion clarifies that incorporation of individual dopants i-e H_2SO_4 and ALS has little effect on crystallinity while their combination (P-Mix) exhibits intense peaks suggesting high crystallinity. The higher crystallinity can be attributed to the smaller dopant such as H_2SO_4 helping in closer chain arrangement while the presence of bulky ALS causes ring distortion in the material [39].

The vibrational bands (Fig. 2b) observed in pristine, doped and binary doped Pani are explained on the basis of normal modes. The contribution from the stretching mode of NH part present in polymer is observed at 3254 cm^{-1}. Band at 2914 cm^{-1} is related to NH^{2+} part in $C_6H_4NH_2^+C_6H_4$– groups [40,41].

The C–N, C=N and C–H stretching vibrations in the polaron framework of Pani appear at 1248 cm^{-1}. The signals observed at 1348 cm^{-1}, 1144 cm^{-1} and 806 cm^{-1} are assigned to the stretching mode of CN part of a secondary aromatic amine, vibrational band of nitrogen quinine and 1,4-substituted aromatic rings, respectively [41].

The characteristic signals at 1555 cm^{-1} and 1469 cm^{-1} in the spectrum of P–N depict the presence of the benzene and quinone ring deformations, respectively [42]. In P–H_2SO_4, P-ALS and P-Mix, shifting of these bands towards higher wavenumber represent the creation of positive charges on the polymer chain, which is a distinctive behavior of doped polymers [43]. The bands at 1631, 1348, and 1144 cm^{-1} disappeared in all the doped samples, revealing effective doping of polymers with the polaron formation ($C–N^+$) [44]. The major characteristic peaks observed at 3206, 1558, 1462, 1295 and 1234 cm^{-1} are similar to the Pani. In P–H_2SO_4, the band observed at 1031 cm^{-1} indicates $NH^+ \cdots SO_3^-$ interaction between polymer and dopant. The peaks detected at 942 and 682 cm^{-1} are allotted to the stretching of O=S=O and S–O group due to the dopant [45].

In P-ALS, the presence of the bands at 2941 cm^{-1} and 2841 cm^{-1} are related to symmetrical and asymmetrical stretching of alkyl substituent of ALS [46]. In P-Mix, similar peaks are observed as in P-ALS but intensity of the peaks is enhanced due to the presence of H_2SO_4. The FT-IR spectra clearly indicate the presence of counter ions of dopants on PANI salts and confirms the formation of emeraldine salt of the polymer.

3. 3: DC conductivity and electronic spectroscopy

The electrical conductivity of pristine, doped and binary doped Pani was measured by four probe technique**.** The values of electrical conductivity fall in the sequence of P–N < P-ALS < P–H_2SO_4 < P-Mix (0.03, 0.22, 0.10 and 1.42 $\Omega^{-1}\,cm^{-1}$). High conductivity is required for ease of electron transfer from CEs to redox electrolyte. P-Mix exhibits highest conductivity amongst the synthesized materials that might be due to the simultaneous addition of both acidic dopants. The presence of these dopants during synthesis provide maximum acidic medium for the polymerization due to which maximum transport of electrons take place consequently resulting in the enhancement of conductivity [30].

The UV spectra of Pani samples, except P–N (Fig. 3a), reveal a similar shape with three absorption bands. P–N shows two distinct absorption bands at 329 nm and 610 nm representing a local charge transfer between a quinoid ring and the adjacent imine-phenylamine unit [47].

The band ranging from 338 to 346 nm relates to the electronic π to π^* transitions centered on the benzenoid rings. The band centered at 418–428 nm belongs to the polaron–π^* transitions indicating the protonation of polymer backbone [48]. The band obtained in NIR region, in the range of 790–822 nm, corresponds to the protonated Pani which confirms the presence of benzenoid and quinoid rings in the conducting emeraldine salt state of Pani. Stronger absorption of this band represents the introduction of dopants into the polymer backbone [49]. On comparison with UV–Vis absorption spectrum of P–N with that of P– H_2SO_4, P-ALS and P-Mix (Fig. 3a), noticeable differences can be seen, suggesting that the nature and size of the counter ions of various dopants are responsible in the creation of different states of doped and binary doped polymers [50].

It is illustrious that notable changes are observed in blue band with various dopants demonstrating that degree of oxidation is different in all spectra [49]. However, the red region band of the

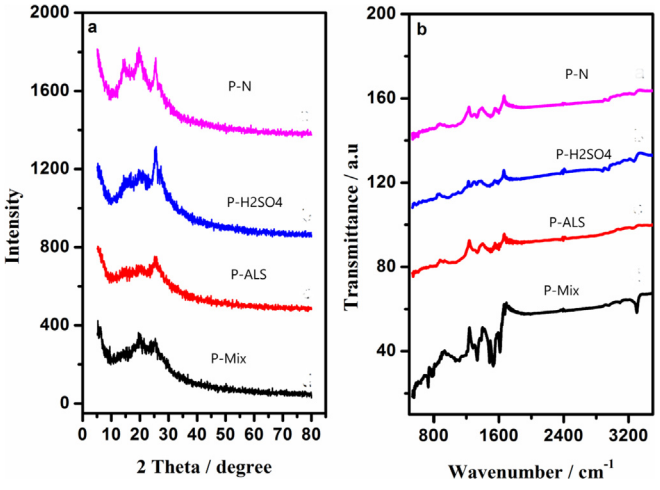

Fig. 2. (a) XRD pattern (b) FTIR spectrum of P–N, P–H_2SO_4, P-ALS and P-Mix.

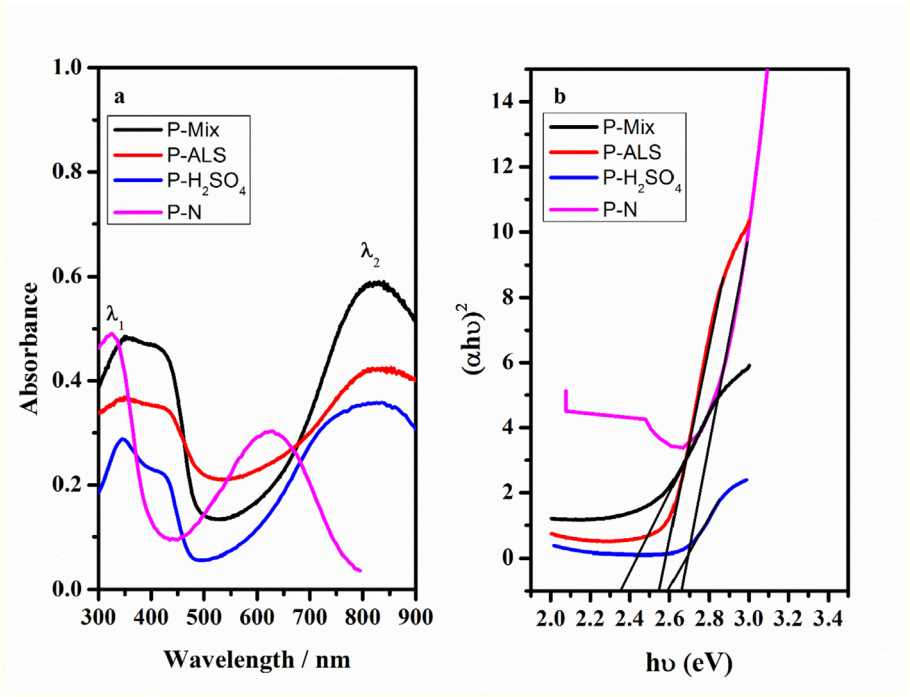

Fig. 3. a) Electronic spectra and b) Tauc plots (showing the band gap energy (Eg), of the synthesized Pani materials, as indicated.

doped and binary doped Pani exhibit a significant red shift compared to P—N, proposing an increase in conjugation length and degree of polymerization of the polymer backbone. This meaningful shift might reveal the effective integration of the dopant ions in the Pani during polymerization which results in the ordered structure of Pani backbone [51].

The absorption band's intensity and wavelength of various Pani samples are presented in Table 2.

The intensity ratio of the low energy band (second band) to the high energy band (first band) (A_2/A_1) for all the samples is presented in Table 2. The A_2/A_1 ratio for P-Mix is larger compared to others indicating the high doping level of the counter anions than the others. It is known that electrical conductivity is directly related to the ordered structure and doping level of Pani backbone [6,52]. The high doping level of P-Mix in comparison with other samples correlates well with the trend in conductivity values as well as crystallinity.

In order to find band gap energy (Eg) of all Pani's, Tauc relation [53] was used to interpret absorption spectra.

$$\alpha h\nu = \mathrm{A}(h\nu - \mathrm{Eg})^{\mathrm{n}}$$

where α is the absorption coefficient and is calculated by the following equation

$$\alpha = \frac{2.303 \times A}{I}$$

where A represents absorbance and I depicted path length.

$h\nu$ is determined by 1240/wavelength. The $(\alpha h\nu)^2$ for direct energy transitions (n = 2) was plotted against the photon energy ($h\nu$) and Eg was determined by extrapolating the slope to $(\alpha h\nu)^2 \rightarrow 0$. Fig. 3 b and Table 2 show that calculated values of Eg are within the range of 2.35—2.67 eV. The band gap values for synthesized materials are also in agreement with the reported works [54].

Table 2
The wavelength (λ), intensity (A) and band gap calculated from the UV—Vis spectrum of different Pani samples.

Sample	A_1	A_2	λ_1	λ_2	A_2/A_1	Eg
P—N	1.13	0.67	329	610	0.59	2.67
P—H2SO4	0.3	0.35	346	790	1.16	2.58
P-ALS	0.36	0,41	344	822	1.21	2.35
P-Mix	0.48	0.58	344	822	1.21	2.35

3.4. Elemental analysis and Mapping

To confirm the presence of different elements and their distribution in the synthesized materials, elemental analysis and mapping was performed with the help of EDX spectroscopy (Fig. 4). Very less amount of sulfur can be seen in the EDX spectrum of P—N (Fig. 4a) which might be due to the presence of APS [40]. For the other electrodes, the detected weights and atomic ratios of sulfur were respectively 3.36% and 1.39% for P—H_2SO_4 (Figs. 4b), 2.58% and 1.07% for P-ALS (Figs. 4c), and 10.46% and 4.64% for P-Mix (Fig. 4d). It shows that P-Mix has the highest content of S, probably due to the presence of two type of dopants (H_2SO_4 and ALS) in the Pani backbone.

3. 5: Electrochemical characterization

Collection of electrons from the external circuit and reduction of iodide species in the electrolyte are main functions of a CE. Therefore, low charge transfer resistance and high catalytic activity are ideal to optimize the efficiency of a CE [55,56]. To explore the electrocatalytic performance of various doped Pani and Pt CEs on I_3^- reduction, CV analysis was performed (Fig. 5 a). All curves show a pair of anodic and cathodic peak corresponding to the redox

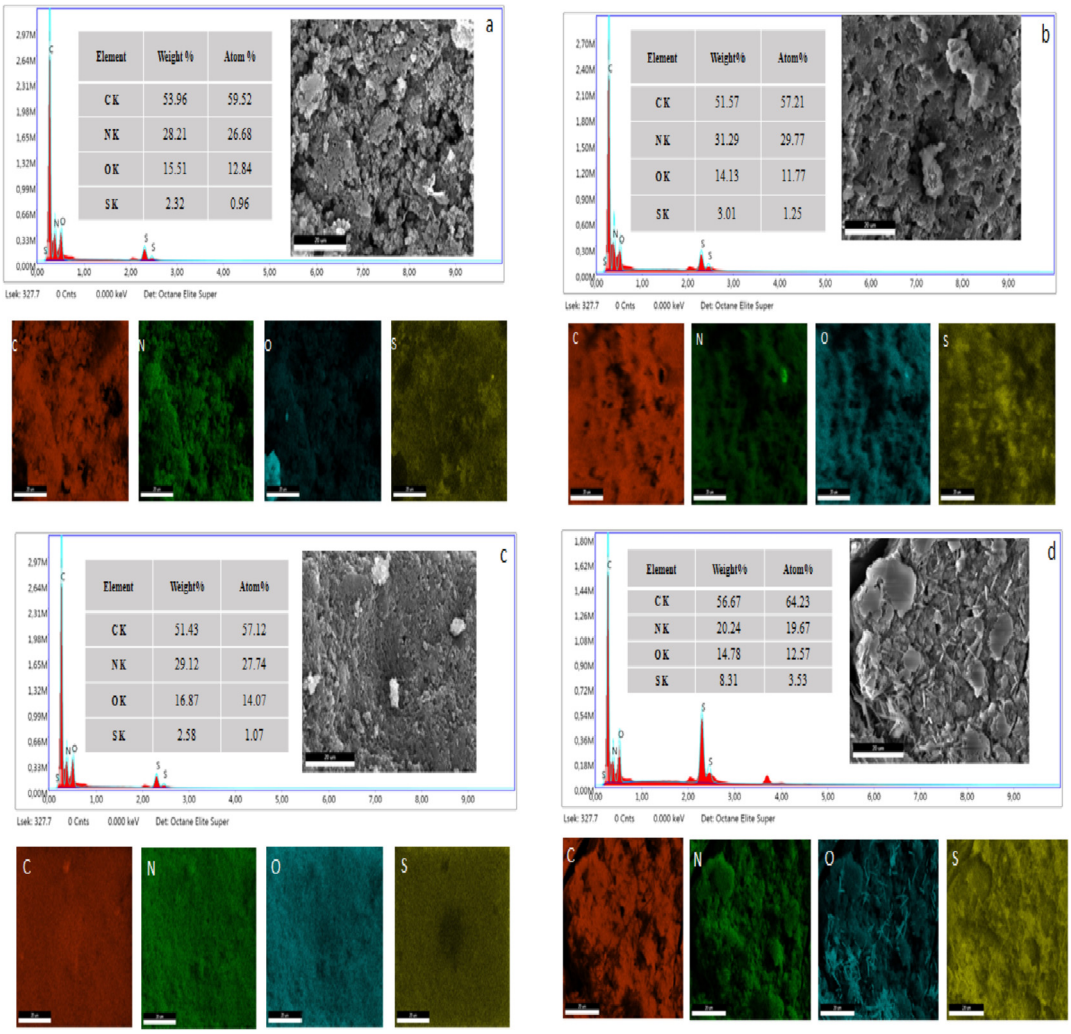

Fig. 4. EDX spectrum and elemental mapping of a) P–N b) P–H_2SO_4 c) P-ALS and d) P-Mix.

reaction of $I_3^- + 2e^- \rightarrow 3\,I^-$, which strongly affects the performance of DSSC [5]. The anodic peak is responsible for the oxidation reaction ($3I^- - 2e^- \rightarrow I_3^-$), and cathodic peak is allotted to the reduction reaction ($I_3^- + 2e^- \rightarrow 3I^-$) [56]. The shape of CV of all the Pani CEs are similar to Pt CE, revealing that Pani CEs have identical electrocatalytic activity towards I- to I_3-redaox couple.

Reduction peak current I_{Red} and peak-to peak separation (Epp) are two critical parameters for comparing the electrocatalytic behavior of various CEs [57]. The values of I_{Red} are in an order of P–N < P–H_2SO_4 < P-ALS < Pt < P-Mix and the Epp values (listed in Table 3) are in an inverse order. Compared with the Pt and other counter electrodes, P-Mix electrode shows higher I_{Red} and lower Epp values for I^-/I_3^- redox reaction. Whereas the low value of I_{Red} is evident in P–N, P–H_2SO_4 and P-ALS. Thus, the simultaneous introduction of H_2SO_4 and ALS into Pani results in a significant improvement in the electrocatalytic activity. Epp is inversely related to rate of charge transfer and high rate of charge transfer is favorable for high electrocatalytic activity of a CE [56]. Further, the smaller △Ep between the redox peaks of I^-/I_3^- with P-Mix 0.59 as compared to Pt electrode (△Ep = 0.25 V) highlights the small polarization overpotential at the surface of P-Mix with remarkable electrochemical activity for I_3^- reduction [21]. The higher I_{Red} is directly related to the dye-regeneration at the photoanode. Generally, in DSSCs, electrons generated from the oxidation of I^- ions to form I_3^-, regenerate photooxidized dyes, and the produced I_3^- ions diffuse to and are reduced at the counter electrode. It is observed that the reduction reaction rate is high in P-Mix electrode, which might enhance the process of dye-regeneration at the photoanode [57,58].

The higher peak current and the lower Epp demonstrate a higher catalytic behavior to I_3^- reduction [7,57]. The trend of electrocatalytic activity of various CEs is in an order of P–N < P–H_2SO_4 < P-ALS < Pt < P-Mix. The trend shows that reduction peak current density of P-Mix is higher than others suggesting high electrocatalytic activity for I_3^- reduction. We can assume that possible high surface area of P-Mix which provide high active sites for reduction of I_3^- [27]. Further, the observed differences in the catalytic activity of the tested electrodes may be affected by different morphologies of the CEs that means different electrode porosity and, thus, different apparent catalytic activities [59].

To elucidate the correlation between diffusion of iodide and peak current density in the binary doped Pani CE, Randles-Sevcik theory was applied to calculate the diffusion coefficient (Dn) [14].

$$\text{Jred} = \text{KAC}\sqrt{n^3 \nu D_n}$$

where K indicates the constant of $2.69^{*}10^5$, n represents the number of electrons transferred in redox reaction, A stands

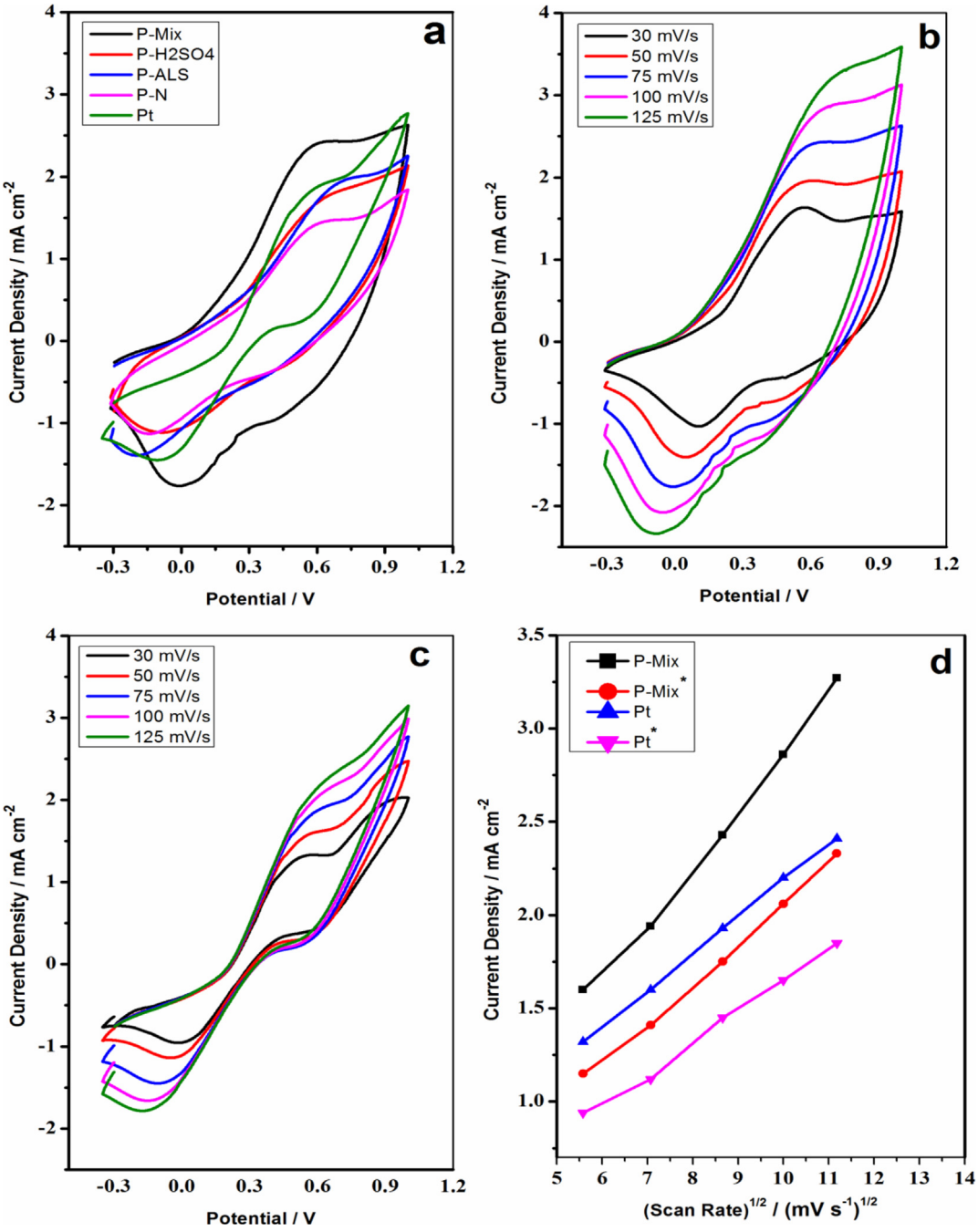

Fig. 5. (a) Cyclic voltammograms of iodide species for Pt and Pani CEs at 50 mV/s scan rate. b and c) CVs of P-Mix and Pt, respectively, at different scan rates (30, 50, 75, 100, 125 mV/s). d) Variation of anodic (P-Mix, Pt) and cathodic (P-Mix*, Pt*) peak current density values with scan rates.

Table 3
CV, J-V, and EIS parameters of DSSCs with P–N, P– H_2SO_4, P-ALS, P-Mix and Pt CEs.

CE	E_{pp} (V)	Dn $\times 10^{-7}$ ($cm^2\ s^{-1}$)	Rs (Ωcm^2)	R_{ct} (Ωcm)	Jsc (mA)	Voc (V)	FF	η (%)
P–N	0.82	0.9×10^{-8}	8.94	23.21	4.71	0.48	0.45	1.14
P–H_2SO_4	0.798	1.45×10^{-8}	6.4	18.17	7.86	0.53	0.43	1.78
P-ALS	0.93	1.70×10^{-7}	4.21	17.16	10.84	0.603	0.43	2.79
P-Mix	0.59	2.3×10^{-7}	4.2	8.26	15.13	0.603	0.53	4.54
Pt	0.69	1.8×10^{-7}	4.6	10.36	12.67	0.64	0.52	4.03

electrode area, and C demonstrates the scan rate and concentration of redox species in bulk, respectively.

As recorded in Table 3, the D_n increases in an order of P–N < P–H_2SO_4 < P-ALS < Pt < P-Mix, for CE's catalytic activity of I_3^-

reduction. It clearly shows that P-Mix CE exhibits larger D_n, which is even slightly larger than Pt electrode. This might be attributed to the facile charge transmission and I_3^- diffusion offered by this electrode [60].

An analysis of electron transfer process was done by recording cyclic voltammograms of Pt and P-Mix as the working electrodes under different scan rates (30–125 mV/s) as illustrated in Fig. 5(b and c). These CV curves illustrated the increase in cathodic and anodic peaks with scan rates. By analyzing the current density and (scan rates)$^{1/2}$ of Pt and P-Mix (Fig. 5d), a linear relationship is observed for both the samples indicating that the redox reaction on the electrodes is controlled by ionic diffusion in the electrolyte [61].

The magnitude of anodic and cathodic peak currents density of P-Mix is higher than that of Pt indicating facile electron transfer. Slope of these linear curves are correlated to the diffusion process, hence estimating the rate of electrochemical reaction. Slope with highest value manifests a high diffusion rate that is beneficial for ease of charge transfer [62]. It can be observed that P-Mix depicts the higher slope than that of Pt. Although Pt CE is the best electrocatalyst but in some cases, electrocatalytic activity of Pt is lower than other CEs. Actually, catalytic activity is intrinsic property of a material but it also depends on the extrinsic factors and can be varied by changing certain extrinsic factors like porosity, particle size, crystal structure, morphology and so on [63].

Dissolution or corrosion of the CE material in electrolytes is major obstacle for its long term stability. In order to check the stability of P-Mix in iodide electrolyte, the freshly prepared P-Mix CE was stored for 30 days and then was subjected to successive CV scanning i-e 15 CV cycles at 50 mVs^{-1}. As illustrated in Fig. 6, no noticeable change is observed in the reduction of current density and peak shifting. This implies that the material is stable and can coexist with iodide species for long period of time [64].

From the above results, we can assume that the improved electrocatalytic activity of P-Mix are due to simultaneous incorporation of ALS and H_2SO_4 in the PANI chain. The combined effect of these two dopants can also be a reason for enhanced conductivity, low bandgap, low charge transfer resistance, as well as the porous microstructure of this material [60,61].

To further elucidate the electron transferability between different counter electrodes and electrolyte, EIS was performed with DSSC based on different counter electrodes. The Nyquists plots (Fig. 7) illustrate impedance characteristics using a well-supported equivalent circuit (shown as an inset in Fig. 7) and are potted in Table 3.

In the equivalent circuit, Rs relates to the ohmic series resistance of the device and is determined directly from the intercept of the real axis at high frequency region. The fill factor of the device is

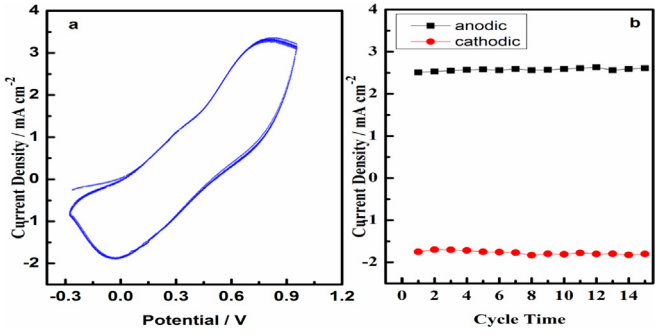

Fig. 6. a) 15 successive CVs of P-Mix electrode, prepared 30 days before performing the experiment, at the scan rate of 50 mVs^{-1} in iodide electrolyte b) Dependence of anodic and cathodic peak current values on cycle time.

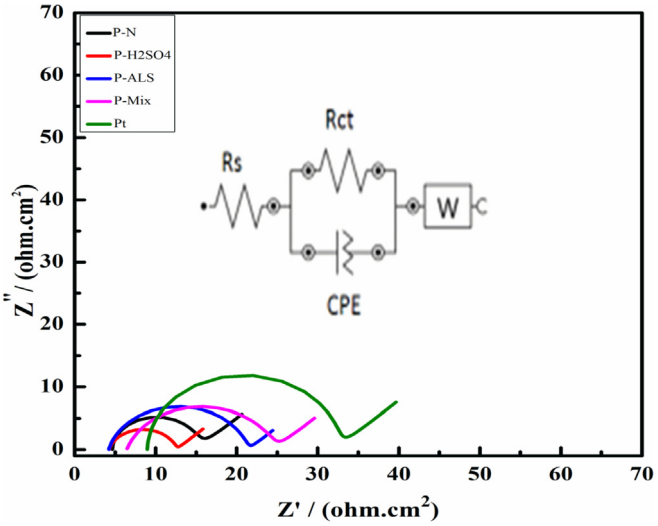

Fig. 7. Nyquist plots of Pt and Pani CEs, as indicated.

mainly dependent on this parameter [60]. Rct observed as a semicircle at high frequency region of Nyquist plot corresponding the charge transfer process at the electrolyte/CE interface, reflecting catalytic activity in the I_3^- reduction at the electrolyte/CE interface and is at the focus of this work. W refers to Warburg impedance which describes the diffusion resistance of electrolyte [21].

P-Mix exhibits much smaller value of W and a higher value of diffusion coefficient. The Rct value decreases in the order of P-Mix (8.26 Ω cm^2) ˃ Pt (10.36 Ω cm^2) ˃ P-ALS (17.16 Ω cm^2) ˃ P– H_2SO_4 (18.17 Ω cm^2) ˃ P–N (23.21 Ω cm^2) signifying an inverse order of electrocatalytic activity. DSSC based on P-Mix CE is found to depict lesser Rct value (8.26 Ω cm^2) compared to that of Pt CE (10.36 Ω cm^2) and its counter parts. The lower Rct value implies that reduction of iodide specie is most favorable at P-Mix CE and performance of this electrode is better than Pt CE. In contrast high R_{CT} values can be recognized to slow ionic diffusion in the structure of Pristine and doped Pani CEs [65]. The lower Rct might be due to the addition of ALS and H_2SO_4 that imparts P-Mix a higher catalytic activity as well as a more porous structure than its counter parts and thereby, the highest device efficiency.

Rct is an important parameter in order to determine the electrochemical stability of a CE in DSSC [64]. Fig. 8 illustrates the electrochemical stability of P-Mix based DSSC which was performed by electrochemical impedance at different time intervals i-e from 0 h to 30 h. Fig. 8 shows that there is slight increase in Rct value with time. The Rct value for fresh cell is 8.26 Ω cm^2 which increases after 5 h to 8.408 Ω cm^2 and to 9.20 after 20 h and then to 9.33 after 30 h while Rs value is not affected with time. This increase in Rct value with time is not so significant suggesting an excellent electrochemical stability of DSSC with P-Mix.

3. 7: Photovoltaic properties

Scheme 2 illustrate the process of photo excitation in the DSSCs [66]. The mesoporous TiO_2 layer (nanometer-sized particles) is coated on a fluorine-doped tin oxide (FTO) glass. TiO_2 film acts as a high surface area support for the sensitizer, provides path for transportation of electron and diffusion of the redox electrolyte. A monolayer of dye (sensitizer) is covalently bonded to the surface of the TiO_2 film. The dye pushes an electron into the CB of mesoporous TiO_2 film by harvesting incident solar light resulting in the

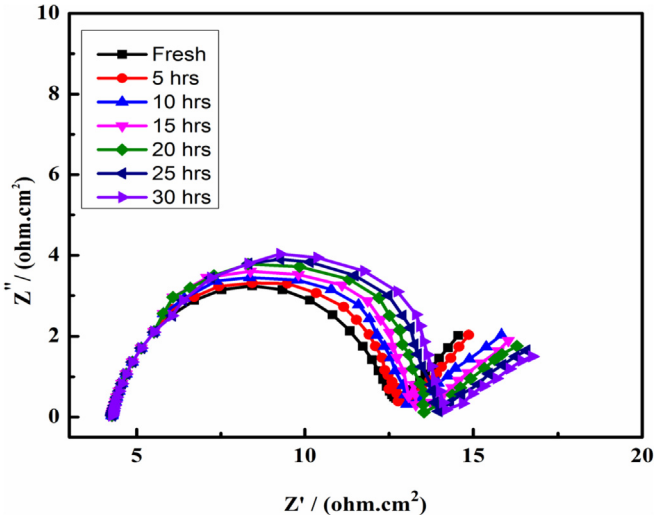

Fig. 8. Stability illustration of DSSC with P-Mix through impedance at 0 V from 0.01-10^5 Hz.

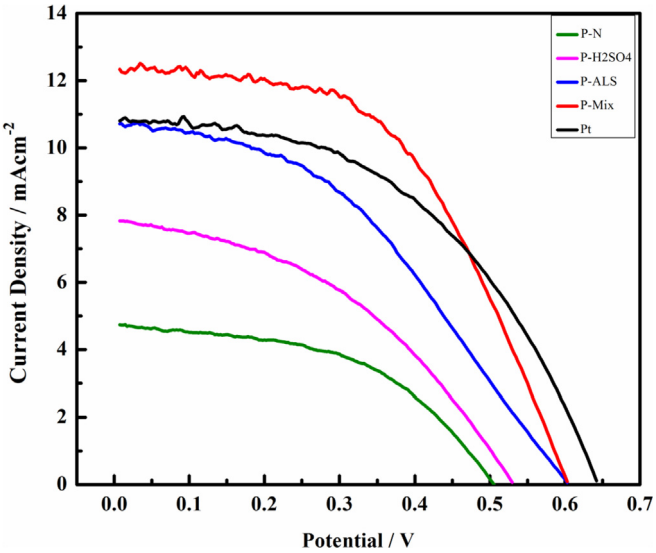

Fig. 9. Photovoltaic performances of DSSCs based on Pt and Pani CEs.

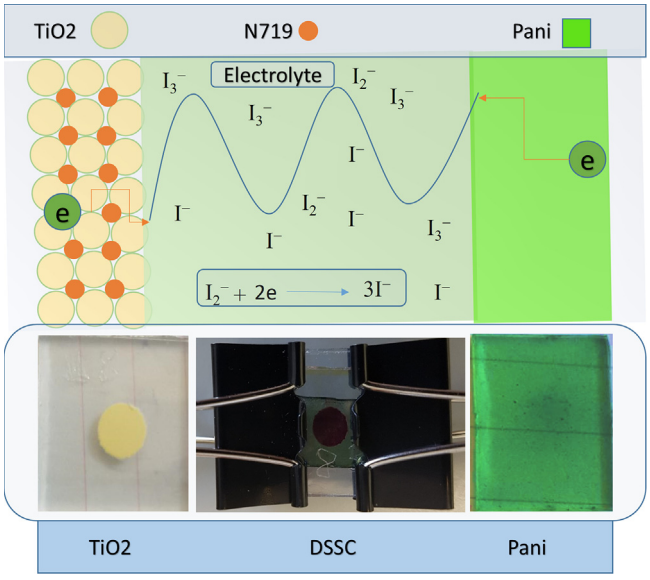

Scheme 2. Schematic representation of DSSC with Pani as CE showing the sequence of electron transfer.

formation of oxidized dye. The regeneration of oxidized dye takes place by triiodide (electron donor) in the electrolyte (charge mediator) as rapidly as possible. The oxidized redox couple (iodide) migrates to the Pani CE and reduced by accepting electrons at CE surface. This results in reduction of oxidation state of doped Pani to emeraldine and/or leucoemeraldine salt. Meanwhile these salts may oxidized by redox couple because of the redox equivalent.

The electrons are collected at CE from the external circuit and return back into the circulation within the cell. The circuit being completed *via* electron migration through the external load.

Fig. 9 shows the J-V characteristics of the DSSCs with Pristine Pani, P– H_2SO_4, P-ALS and P-Mix CEs, with the Pt CE for comparing, under light source of 100 W. The parameters derived from J-V curves are summarized in Table 3. Eqs. (1) and (2) are used to calculate the fill factor (FF) and power conversion efficiency (η) of the DSSCs, respectively [67].

$$FF = \frac{V_{max} \times J_{max}}{V_{oc} \times J_{sc}} \quad (1)$$

$$\eta = \frac{V_{oc} \times J_{sc} \times FF}{Pin} \quad (2)$$

According to the experimental data, the poor performance of P–N CE based DSSC in terms of the lowest values of η = 1.14%, Voc = 0.48 mV and FF = 0.45 might be due to the fact that this CE has insufficient surface area for diffusion of redox species. This may increase the chances of recombination between the photoinjected electrons and iodide ions at the CE [65, 67]. The P– H_2SO_4 also demonstrate low value of η representing that H_2SO_4 alone is not sufficient to improve the photocatalytic properties of the material.

A noticeable difference is observed in Jsc and Voc of P-ALS based DSSC. This might be due to doping of Pani with ALS that can enhance the conductivity and desirable morphology of counter electrodes. The efficiency of P-ALS increases to 2.79%. In the P-Mix, the value of FF increases noticeably with improved Jsc and Voc values; increasing its performance to 4.54%, a level more efficient than that of DSSCs with Pt CEs (4.03%). As aforementioned, high conductivity and low charge transfer resistance due to contribution of binary dopants in P-Mix are attributed to the higher value of Jsc, leading to high catalytic activity for facile reduction of electrolyte at the CEs. In addition, the increased electro-catalytic ability for fast reduction of I_3^- ions at the P-Mix CEs results in the reduced availability of I_3^- ions for recombination with photoinjected electrons, resulting in higher Voc compared to the other CEs [68,69].

The improvement in the Jsc can be attributed to the fact that simultaneous doping of P-Mix with H_2SO_4 and ALS increases the conductivity and provide unusual morphology to Pani CE which may bring more active sites for I_3^- reduction. These active sites are responsible for serving a good path for transportation of charges [60,70].

3. 8: Multiple start/stop proficiency

When applied as roof panels, portable sources or windows, the solar panels should be expected to have advantages of numerous start/stop proficiency, fast start-stop performance, and insistent stability. By alternatively darkening (0 mWcm^{-2}) and illuminating

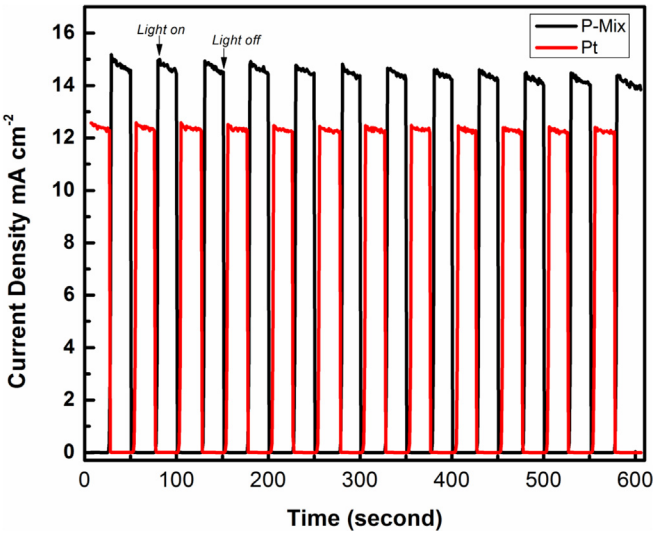

Fig. 10. The start-stop switch by alternatively irradiating (100 mW cm^{-2}) and darking (0 mW cm^{-2}) the cell device based on P-Mix and Pt as CEs at an internal of 25 s and 0 V.

(100 mWcm^{-2}) the P-Mix CE based DSSC, the start/stop switches were recorded to estimate the start-up performance. The performance of DSSC/Pt is also examined for comparison. As shown in Fig. 10, a rapid increase in photocurrent density under irradiation with no time delay depicts a fast start-up behavior. After twelve start-stop cycles, the photocurrent density is still unaffected in comparison to its initial state. This confirms a rapid light response and hence high electrocatalytic activity towards redox electrolyte. About 96% of the initial photocurrent density was measured after eleven cycles as compared to Pt based DSSC having 93%, implying a superior capability of the P-Mix CE to start multiple times, which is a necessity for a durable solar panel [65].

Conclusions

In summary, we have established the simple preparation of P–N, P–H_2SO_4, P-ALS and P-Mix CEs on the FTO substrate for energy harvesting in DSSC. The electrochemical characterization demonstrates that, compared to H_2SO_4, ALS is more effective to enhance the electrochemical and electrocatalytic activities of Pani. By integrating H_2SO_4 and ALS simultaneously with Pani, the P-Mix exhibits further improved electrocatalytic activity and charge transfer ability for the reduction of I^{3-} due to its high cathodic current density and the low R_{CT}. The DSSC assembled by P-Mix CE with a thickness of 8 μm provides superior power conversion efficiency compared to that of Pt CE. Moreover, the virtues on fast start–up and multiple start/stop capability motivate the potential applications of such flexible DSSCs in movable power sources and photovoltaic curtain walls. In view of this facile approach, low-cost, and highly electrochemical catalysts, the P-Mix CE demonstrates a promising potential in production of DSSCs.

Acknowledgments

The Engineering and Physical Science Research Council, UK (EPSRC grant No EP/P510956/1 and EP/R512801/1), Alexander von Humboldt Foundation, Germany, and Higher Education Commission Pakistan (project No. 20–1647 & 20–3111/NRPU/R&D/HEC) are highly acknowledged for financial support. NSG Pilkington Glass Ltd. is acknowledged for kindly providing the FTO substrates for this work. Dr.-Ing. Ingo Kampen and Ms Louise Niemeyer, Institute für Partikeltechnik, TU Braunschweig Germany are also acknowledged for their kind support in SEM and EDX measurements.

References

[1] R. Tas, M. Can, S. Sonmezoglu, Exploring on photovoltaic performance of dye-sensitized solar cells using polyaniline as a counter electrode: role of aluminum-solvent interactions, IEEE J Photovolt 7 (2017) 792–801.
[2] S. Yun, Y. Zhang, Q. Xu, J. Liu, Y. Qin, Recent advance in new-generation integrated devices for energy harvesting and storage, Nano Energy 60 (2019) 600–619.
[3] A. Knotta, O. Makarovskiya, J. O'Sheaa, Y. Wub, C. Tuck, Scanning photocurrent microscopy of 3D printed light trapping structures in dye-sensitized solar cells, Sol. Energy Mater. Sol. Cells 180 (2018) 103–109.
[4] P. Selvaraj, H. Baig, H, T.K. Mallick, J. Siviter, A. Montecucco, W. Li, M. Paul, T. Sweet, M. Gao, A.R. Knox, S. Sundaram, Enhancing the efficiency of transparent dye-sensitized solar cells using concentrated light, Sol. Energy Mater. Sol. Cells 175 (2018) 29–34.
[5] G. Yue, J. Wu, Y. Xiao, J. Lin, M. Huang, Flexible solar cells based on PCBM/P3HT heterojunction, Front. Optoelectron. China 4 (2011) 108–113.
[6] S. Wang, S. Lu, X. Li, X. Zhang, S. He, T. He, Study of H_2SO_4 concentration on properties of H_2SO_4 doped polyaniline counter electrodes for dye-sensitized solar cells, J. Power Sources 242 (2013) 438–446.
[7] A.A. Arbab, K.C. Sun, I.A. Sahito, A.A. Memon, Y.S. Choi, S.H. Jeong, Fabrication of textile fabric counter electrodes using activated charcoal doped multi walled carbon nanotube hybrids for dye sensitized solar cells, J. Mater. Chem. A. 4 (2016) 1495–1505.
[8] H. Wang, Y.H. Hu, Graphene as a counter electrode material for dye-sensitized solar cells, Energy Environ. Sci. 5 (2012) 8182–8188.
[9] B. Lu, Z. Xiao, H. Zhu, W. Xiao, W. Wu, D. Wang, Enhanced capacitive properties of commercial activated carbon by re-activation in molten carbonates, J. Power Sources 298 (2015) 74–82.
[10] A. Aboagye, H. Elbohy, A.D. Kelkar, Q. Qiao, J. Zai, X. Qian, L. Zhang, Electrospun carbon nanofibers with surface-attached platinum nanoparticles as cost-effective and efficient counter electrode for dye-sensitized solar cells, Nano Energy 11 (2015) 550–556.
[11] Y. Xiao, G. Han, Y. Li, M. Li, J.Y. Lin, Three-dimensional hollow platinum–nickel bimetallic nanoframes for use in dye-sensitized solar cells, J. Power Sources 278 (2015) 149–155.
[12] Y. Xiao, J. Wu, J.Y. Lin, S.Y. Tai, G. Yue, Pulse electrodeposition of CoS on MWCNT/Ti as a high performance counter electrode for a Pt-free dye-sensitized solar cell, J. Mater. Chem. A. 1 (2013) 1289–1295.
[13] H.M. Chuang, C.T. Li, M.H. Yeh, C.P. Lee, R. Vittal, K.C. Ho, A coral-like film of Ni@NiS with core–shell particles for the counter electrode of an efficient dye-sensitized solar cell, J. Mater. Chem. A. 2 (2014) 5816–5824.
[14] S. Yun, Y. Qin, A.R. Uhl, N. Vlachopoulos, M. Yin, D. Li, X. Han, A. Hagfeldt, New-generation integrated devices based on dye-sensitized and perovskite solar cells, Energy Environ. Sci. 11 (2018) 476–526.
[15] S. Yun, J.N. Freitas, A.F. Nogueira, Y. Wang, S. Ahmad, Z.S. Wang, Dye-sensitized solar cells employing polymers, Prog. Polym. Sci. 59 (2016) 1–40.
[16] Y. Xiao, G. Han, Y. Li, M. Li, Y. Chang, High performance of Pt-free dye-sensitized solar cells based on two-step electropolymerized polyaniline counter electrodes, J. Mater. Chem. A. 2 (2014) 3452–3460.
[17] M.A. Bavio, G.G. Acosta, T. Kessler, Synthesis and characterization of polyaniline and polyaniline -carbon nanotubes nanostructures for electrochemical supercapacitors, J. Power Sources 245 (2014) 475–481.
[18] S. Virji, J. Huang, R.B. Kaner, B.H. Weiller, Polyaniline nanofiber gas sensors: examination of response mechanisms, Nano Lett. 4 (2004) 491–496.
[19] K. Zhou, Y. He, Q. Xu, Q. Zhang, A. Zhou, Z. Lu, L.K. Yang, Y. Jiang, D. Ge, X.Y. Liu, H. Bai, A hydrogel of ultrathin pure polyaniline nanofibers: oxidant-templating preparation and supercapacitor application, ACS Nano 12 (2018) 5888–5894.
[20] S. Yun, A. Hagfeldt, T. Ma, Pt-free counter electrode for dye-sensitized solar cells with high efficiency, Adv. Mater. 26 (2014) 6210–6237.
[21] T. Zhang, S. Yun, X. Li, X. Huang, Y. Hou, Y. Liu, J. Li, X. Zhou, W. Fang, Fabrication of niobium-based oxides/oxynitrides/nitrides and their applications in dye-sensitized solar cells and anaerobic digestion, J. Power Sources 340 (2017) 325–336.
[22] K. Lee, S. Cho, S. Heum Park, A.J. Heeger, C.W. Lee, S.H. Lee, Metallic transport in polyaniline, Nature 441 (2006) 65.
[23] K.H. Lee, B.J. Park, D.H. Song, I.J. Chin, H.J. Choi, The role of acidic m-cresol in polyaniline doped by camphorsulfonic acid, Polymer 50 (2009) 4372–4377.
[24] J. Xing, M. Liao, C. Zhang, M. Yin, D. Li, Y. Song, The effect of anions on the electrochemical properties of polyaniline for supercapacitors, Phys. Chem. Chem. Phys. 19 (2017) 14030–14041.
[25] S. Yun, Y. Liu, T. Zhanga, S. Ahmad, Recent advances in alternative counter electrode materials for Co-mediated dye-sensitized solar cells, Nanoscale 7 (2015) 11877–11893.
[26] S. Sharma, S. Bulkesh, S.K. Ghoshal, D. Mohan, Dye sensitized solar cells: from genesis to recent drifts, Renew. Sustain. Energy Rev. 70 (2017) 529–537.
[27] Sining Yun, * Hong Zhang, Huihai Pu, Junhong Chen, Anders Hagfeldt , and Tingli Ma metal oxide/Carbide/carbon nanocomposites: in situ synthesis,

characterization, calculation, and their application as an efficient counter electrode catalyst for dye-sensitized solar cells, Adv. Energy Mater. 3 (2013) 1407–1411.
[28] N. Elakhya, G. Gayatri, S. Aparna, P. Rajesh, P. Ramasamy, Effect of tin oxide crystallite size on the efficacy of polyaniline-tin oxide nanocomposite based counter electrode for DSSC applications, Optik 142 (2017) 436–445.
[29] S.S. Jeon, C. Kim, T.H. Lee, Y.W. Lee, K. Do, J. Ko, S.S. Im, Camphorsulfonic acid doped polyaniline transparent counter electrode for dye-sensitized solar cells, J. Phys. Chem. C 116 (2012) 22743–22748.
[30] Y. Gawli, A. Banerjee, D. Dhakras, M. Deo, D. Bulani, P. Wadgaonkar, M. Shelke, S. Ogale, 3D polyaniline architecture by concurrent inorganic and organic acid doping for superior and robust high rate supercapacitor performance, Sci. Rep. 6 (2016) 1–10.
[31] P. Yang, J. Duan, D. Liu, Q. Tang, B. He, Multi-interfacial polyaniline-graphene/platinum counter electrodes for dye-sensitized solar cells, Electrochim, Acta 173 (2015) 331–337.
[32] B. He, Q. Tang, T. Liang, Q. Li, Efficient dye-sensitized solar cells from polyaniline–single wall carbon nanotube complex counter electrodes, J. Mater. Chem. A. 2 (2014) 3119–3126.
[33] A. Khosrozadeh, M.A. Darabi, M. Xing, Q. Wang, Flexible electrode design: fabrication of freestanding Polyaniline based composite films for high-performance supercapacitors, ACS Appl. Mater. Interfaces 8 (2016) 11379–11389.
[34] Y. Zhang, S. Yun, C. Wang, Z. Wang, F. Han, Y. Si, Bio-based carbon-enhanced tungsten-based bimetal oxides as counter electrodes for dye-sensitized solar cells, J. Power Sources 423 (2019) 339–348.
[35] T. Yu, P. Zhu, Y. Xiong, H. Chen, S. Kang, H. Luo, S. Guan, Synthesis of micro-spherical polyaniline/graphene composites and their application in super-capacitors, Electrochim. Acta 222 (2016) 12–19.
[36] P. Chal, A. Shit, A.K. Nandi, Dye-sensitized solar cell from a new organic n-type semiconductor/polyaniline composite: insight from impedance spectroscopy, J. Mater. Chem. C. 4 (2016) 272–285.
[37] G. Han, M. Wang, D. Li, J. Bai, G. Dia, Novel upconversion Er, Yb-CeO2 hollow spheres as scattering layer materials for efficient dye-sensitized solar cells, Sol. Energy Mater. Sol. Cells 160 (2017) 54–59.
[38] M.O. Ansari, F. Mohammad, Thermal stability and electrical properties of dodecyl-benzene-sulfonic-acid doped nanocomposites of polyaniline and multi-walled carbon nanotubes, Compos. B Eng. 43 (2012) 3541–3548.
[39] S. Yun, H. Pu, J. Chen, A. Hagfeldt, T. Ma, Enhanced performance of supported HfO_2 counter electrodes for redox couples used in dye-sensitized solar cells, ChemSusChem 7 (2014) 442.
[40] S. Palaniappan, V. Nivasu, Emulsion polymerization pathway for preparation of organically soluble polyaniline sulfate, New J. Chem. 26 (2002) 1490–1494.
[41] J. Amalraj, P. Srinivasan, D. David, P. Adam, One-step preparation of solution processable conducting polyaniline by inverted emulsion polymerization using didecyl ester of 4-sulfophthalic acid as multifunctional dopant, J. Polym. Sci. A. 46 (2008) 1051–1057.
[42] M.V. Kulkarni, A.K. Viswanath, Spectroscopic, thermal and electrical properties of sulphonic acids doped poly (o-anisidine) and their application as humidity sensor, Sens. Actuators B Chem. 107 (2005) 791–797.
[43] A.F. Baldissera, K. L. d. Miranda, C. Bressy, C. Martin, A. Margaillan, C.A. Ferreira, Using conducting polymers as active agents for marine anti-fouling paints, Math. Res. 18 (2015) 1129–1139.
[44] F. Zeng, Z. Qin, B. Liang, T. Li, N. Liu, M. Zhu, Polyaniline nanostructures tuning with oxidants in interfacial polymerization system, Pro Nat Sci-Mater. 25 (2015) 512–519.
[45] T. Chen, C. Dong, X. Li, J. Gao, Thermal degradation mechanism of dodecylbenzene sulfonic acid- hydrochloric acid co-doped polyaniline, Polym. Degrad. Stab. 94 (2009) 1788–1794.
[46] S.B. Sydulu, S. Palaniappan, P. Srinivas, Nano fibre polyaniline containing long chain and small molecule dopants and carbon composites for supercapacitor, Electrochim. Acta 95 (2013) 251–259.
[47] Y. Xie, X. Sha, Electrochemical cycling stability of nickel (II) coordinated polyaniline, Synth. Met. 237 (2018) 29–39.
[48] M. Shi, Y. Zhang, M. Bai, B. Li, Facile fabrication of polyaniline with coral-like nanostructure as electrode material for supercapacitors, Synth. Met. 233 (2017) 74–78.
[49] W. Wang, A.G. MacDiarmid, New synthesis of phenyl/phenyl end-capped tetraaniline in the leucoemeraldine and emeraldine oxidation states, Synth. Met. 129 (2002) 199–205.
[50] O.N. Paul-Nwokocha, J.O. Ozuomba, Synthesis and optical characterization of acid-doped polyaniline thin films, Nigerian J. Technol. 37 (2018) 135.
[51] F. Zeng, Z. Qin, B. Liang, T. Li, N. Liu, M. Zhu, Polyaniline nanostructures tuning with oxidants in interfacial polymerization system, Pro, Nat. Sci. Mater. 25 (2015) 512–519.
[52] E. Lahiff, T. Woods, W. Blau, G.G. Wallace, D. Diamond, Synthesis and characterization of controllably functionalized polyaniline nanofibres, Synth. Met. 159 (2009) 741–748.
[53] K.T. Vadiraj, S.L. Belagali, Characterization of polyaniline for optical and electrical properties, IOSR-J. Applied Chem. 8 (2015) 53–56.
[54] S. Chaturvedi, R. Das, P. Poddar, S. Kulkarni, Tunable band gap and coercivity of bismuth ferrite–polyaniline core–shell nanoparticles: the role of shell thickness, RSC Adv. 5 (2015) 23563–23568.
[55] S. Yun, A. Hagfeldt, T. Ma, Superior catalytic activity of sub-5 mm-thick Pt/SiC films as counter electrodes for dye-sensitized solar cells, ChemCatChem 6 (2014) 1584.
[56] C.T.T. Thuy, J.H. Jung, S. Thogiti, W.S. Jung, K.S. Ahn, J.H. Kim, Graphene coated alumina-modified polypyrrole composite films as an efficient Pt-free counter electrode for dye-sensitized solar cells, Electrochim. Acta 205 (2016) 170–177.
[57] Y. Xiao, J.Y. Lin, J. Wu, S.Y. Tai, G. Yue, T.W. Lin, Dye-sensitized solar cells with high-performance polyaniline/multi-wall carbon nanotube counter electrodes electropolymerized by a pulse potentiostatic technique, J. Power Sources 233 (2013) 320–325.
[58] S. Yasuteru, K. Takayuki, W. Yuji, Y. Shozo, Application of poly(3,4-ethylenedioxythiophene) to counter electrode in dye-sensitized solar cells, Chem. Lett. 31 (2002) 1060–1061.
[59] J.G. Rowley, B.H. Farnum, S. Ardo, G.J. Meyer, Iodide chemistry in dye-sensitized solar cells: making and breaking I–I bonds for solar energy conversion, J. Phys. Chem. Lett. 1 (2010) 3132–3140.
[60] Y. Liu, S. Yun, X. Zhou, Y. Hou, T. Zhang, J. Li, A. Hagfeldt, Intrinsic origin of superior catalytic properties of tungsten-based catalysts in dye-sensitized solar cells, Electrochim. Acta 242 (2017) 390–399.
[61] P. Sudhagar, S. Nagarajan, Y.G. Lee, D. Song, T. Son, W. Cho, M. Heo, K. Lee, J. Won, Y.S. Kang, Synergistic catalytic effect of a composite (CoS/PEDOT:PSS) counter electrode on triiodide reduction in dye-sensitized solar cells, ACS Appl. Mater. Interfaces 3 (2011) 1838–1843.
[62] Q. Qi, T. Jie, Y. Yan, D. Xiang, In situ oxidative polymerization of polyaniline counter electrode on ITO conductive glass substrate, Polym. Eng. Sci. 51 (2011) 663–669.
[63] S. Yun, M. Wu, Y. Wang, J. Shi, X. Lin, A. Hagfeldt, T. Ma, Pt-like behavior of high-performance counter electrodes prepared from binary tantalum compounds showing high electrocatalytic activity for dye-sensitized solar cells, ChemSusChem 6 (2013) 411–416.
[64] S. Yun, P.D. Lund, A. Hinsch, Stability assessment of alternative platinum free counter electrodes for dye-sensitized solar cells, Energy Environ. Sci. 8 (2015) 3495–3514.
[65] A. Ramar, R. Saraswathi, A.T.E. Vilian, S.-M. Chen, F.M. Wang, Poly-isothianaphthene/graphene nanocomposite as a new counter electrode material for high performance dye sensitized solar cell, Synth. Met. 230 (2017) 58–64.
[66] J. Wu, Z. Lan, J. Lin, M. Huang, Y. Huang, L. Fan, G. Luo, Y. Lin, Y. Xie, Y. Wei, Counter electrodes in dye-sensitized solar cells, Chem. Soc. Rev. 46 (2017) 5975–6023.
[67] K. Wu, L. Chen, W. Cui, B. Ruan, M. Wu, The effect of transition metal ions ($M^{2+} = Mn^{2+}$, Ni^{2+}, Co^{2+}, Cu^{2+}) on the chemical synthesis polyaniline as counter electrodes in dye-sensitized solar cells, Chin, J. Chem. Eng. 25 (2017) 671–675.
[68] C.H. Tsai, W.C. Huang, Y.C. Hsu, C.J. Shih, I.J. Teng, Y.H. Yu, Poly(o-methoxyaniline) doped with an organic acid as cost-efficient counter electrodes for dye-sensitized solar cells, Electrochim. Acta 213 (2016) 791–801.
[69] S. Cho, S.H. Hwang, C. Kim, J. Jang, Polyaniline porous counter-electrodes for high performance dye-sensitized solar cells, J. Mater. Chem. 22 (2012) 12164–12171.
[70] X. Chen, J. Liu, K. Qian, J. Wang, Ternary composites of Ni–polyaniline–graphene as counter electrodes for dye-sensitized solar cells, RSC Adv. 8 (2018) 10948–10953.